Journal of Solid State Chemistry 316 (2022) 123635

Contents lists available at ScienceDirect

Journal of Solid State Chemistry

journal homepage: www.elsevier.com/locate/jssc

Narrowing the tolerance factor limits for hybrid organic-inorganic dicyanamide-perovskites

Javier García-Ben [a,b], Alberto García-Fernández [c], Pedro Dafonte-Rodríguez [a,b], Ignacio Delgado-Ferreiro [a,b], Ute B. Cappel [c], Socorro Castro-García [a,b], Manuel Sánchez-Andújar [a,b,**], Juan Manuel Bermúdez-García [a,b,***], María Antonia Señarís-Rodríguez [a,b,*]

[a] Universidade da Coruña, Quimolmat, Centro de Investigacións Científicas Avanzadas (CICA), Rúa as Carballeiras, 15071, A Coruña, Spain
[b] Universidade da Coruña, Quimolmat, Departamento de Química, Facultade de Ciencias, Campus da Zapateira, 15008, A Coruña, Spain
[c] Division of Applied Physical Chemistry, Department of Chemistry, KTH Royal Institute of Technology, SE-100 44, Stockholm, Sweden

ARTICLE INFO

Keywords:
Hybrid organic-inorganic perovskites
Tolerance factor
Dicyanamide compounds
A-cation volume
Promolecule isosurface

ABSTRACT

In this work we focus in setting the limits of the tolerance factor and the size of the A-cations that stabilize the perovskite structure in hybrid dicyanamide compounds [A][Mn(dca)$_3$]. For this purpose, we propose an alternative, simple approach to calculate a more realistic effective ionic radius for the large and anisotropic A-cations often present in these type of compounds. We test the proposed procedure by analysing the crystal structures of [A][Mn(dca)$_3$] dicyanamide hybrids reported in the literature and recalculating the tolerance factors of such compounds, as well as by preparing five new [A][Mn(dca)$_3$] members, discussing also the influence of the A-cation shape in the stability limits of the perovskite structure. Interestingly, such methodology is not only useful to develop new compounds of the emerging family of (multi)functional multi(stimuli)-responsive dicyanamide materials but can also be applied to other hybrid organic-inorganic perovskites and related materials.

1. Introduction

One of the foremost goals in Solid State and Materials Chemistry is the design and prediction of new solid-state materials with interesting functional properties, for the development of new technologies that allow to better face the pressing challenges of current society. But materials design is a complex and sometimes even frustrating task, resource intensive and time consuming.

In that context, during the last decades, much effort has been devoted to accelerate materials discovery, such as the use of data repositories, automation with robotics and, above all, parallelisation and computational resources [1].

Also, more traditional semi-empirical rules that are extracted from experimental facts of series of compounds are still highly effective to guide the prediction and design of new materials, in particular with given crystal structures [2]. In this context, Goldschmidt's tolerance factor (t) has been successfully used during the last century to predict the stability of ABX_3 compounds [3], specially mixed oxides, with perovskite structure, many of them with very outstanding properties (ferroelectricity, high superconductivity, magnetoresistance, etc.).

As it is well-known, the tolerance factor is essentially a geometrical parameter which relates the size of the cations in the A- and B-sites to that of the anions in the X-site, through Eq. (1):

$$t = \frac{r_A + r_X}{\sqrt{2}\,(r_B + r_X)} \quad (1)$$

In this model, the involved inorganic ions are considered as hard spheres with ionic radii of r_A, r_B and r_X for the A-, B- and X sites, respectively. This simple —but very effective— relationship can be used to easily predict the formation of inorganic perovskites from different combinations of A, B and X ions. For values of t = [0.8–1], it is found that the selected combination will have a high probability of forming a perovskite structure. This structure is expected to display a cubic symmetry for t = [0.9–1], while structural distortions —specifically the octahedra tiltings described by Glazer [4]— are expected for t = [0.8–0.89]. Tolerance factors outside this range will lead to different

* Corresponding author. Universidade da Coruña, Quimolmat, Centro de Investigacións Científicas Avanzadas (CICA), Rúa as Carballeiras, 15071, A Coruña, Spain.
** Corresponding author. Universidade da Coruña, Quimolmat, Centro de Investigacións Científicas Avanzadas (CICA), Rúa as Carballeiras, 15071, A Coruña, Spain.
*** Corresponding author. Universidade da Coruña, Quimolmat, Centro de Investigacións Científicas Avanzadas (CICA), Rúa as Carballeiras, 15071, A Coruña, Spain.
E-mail addresses: m.andujar@udc.es (M. Sánchez-Andújar), j.bermudez@udc.es (J.M. Bermúdez-García), m.senaris.rodriguez@udc.es (M.A. Señarís-Rodríguez).

https://doi.org/10.1016/j.jssc.2022.123635
Received 28 June 2022; Received in revised form 23 September 2022; Accepted 28 September 2022
Available online 1 October 2022

structural topologies, such as ilmenite (for $t < 0.8$) or hexagonal structures ($t > 1$).

In 2014, Kieslich et al. extended the tolerance factor approach to predict the stability of the perovskite structure among members of the emergent family of dense hybrid organic-inorganic compounds with ABX_3 stoichiometry [5–7]. The resulting materials, which are known as hybrid organic-inorganic perovskites (HOIPs), integrate organic and inorganic building-blocks in the structure, namely: organic cations (normally alkylamine or alkylphosphone cations) in the A-site, metal cations in the B site and either halides or organic/inorganic polyatomic bidentate-bridging ligands in the X-site [8]. Depending on X, different families of HOIPs arise such as azide, formate, halide, thiocyanate, dicyanamide, perchlorate, hypophosphite, tetrafluoroborate or borohydride perovskites [8–10]. In the last years some of these HIOPs have attracted a lot of attention due to their outstanding functional properties such as photovoltaic [11,12], ferroelectric [13], or barocaloric behaviour [14–16].

This explains the relevance of having a powerful and simple guiding principle to predict which combination of A, B and X ions will lead to the formation of HOIPs and the great enthusiasm with which the extended tolerance factor was received by the scientific community.

In the Kieslich et al. proposed model to estimate such extended tolerance factor (illustrated in Fig. 1), it is assumed that the organic A-cations are rigid spheres, independently of their real shape, with rotational freedom around their centre of mass, and with an effective radii (r_{Aeff}) equivalent to Eq. (2):

$$r_{Aeff} = r_{mass} + r_{ion} \tag{2}$$

In this expression r_{mass} is calculated using single crystal X-ray diffraction data as the distance between the centre of mass and the furthest atom from this centre (excluding hydrogen atoms), and r_{ion} is the corresponding ionic radius of this furthest atom [5]. In a similar way, X-anions are treated as rigid cylinders with effective radius (r_{Xeff}) and effective height (h_{Xeff}).

These parameters are then included in the extended Goldschmidt's tolerance factor for HOIPs, α, in Eq. (3):

$$\alpha = \frac{r_{Aeff} + r_{Xeff}}{\sqrt{2}\,(r_B + 0.5\,h_{Xeff})} \tag{3}$$

Most interestingly, despite its simplicity, the extended tolerance factor identifies a stability window α = [0.8–1], where hybrid organic-inorganic compounds with ABX_3 stoichiometry are expected to exhibit the perovskite structure [5].

tThis approach has been very successful for hybrid perovskites with short polyatomic X-anions, such as azides, formates, cyanides or borohydrides [6]. Nevertheless, it also has some limitations, especially when there is an important covalent contribution to the B-X bonds [9] or when rather large and anisotropic A cations and long X ions are present in the structure. This second problematic is found, for example, in the case of dicyanamide (dca = $[N(CN)_2]^-$) perovskites with general formula $[A][M(dca)_3]$.

In those $[A][M(dca)_3]$ HOIPs, the presence of the relatively large dca bridging ligand gives rise to perovskites with unprecedent structural degrees of freedom, that in turn allow for a large chemical diversity of polyatomic cations that can be accommodated in the A-site. As a result, this family has been expanding in the last years, and at present about 32 $[A][M(dca)_3]$ HOIPs are already known, in which A are rather large monovalent organic cations (typically alkylammonium or alkylphosphonium cations) and M are Mn^{2+}, Fe^{2+}, Co^{2+}, Ni^{2+} and Cd^{2+} divalent metal cations [17]. It has be found that some of those dicyanamide HOIPs already show very remarkable barocaloric, ferroelastic or weak-ferromagnetic properties [18–25]. Hence, there is a marked interest in having tools, such the predictions of the stability using the extended tolerance factor, to help design and prepare new members of this promising family.

Nevertheless, and as mentioned above, the extended tolerance factor approach does not seem to be very accurate for such $[A][M(dca)_3]$ perovskites, since the calculated α values for the existing ones are in the range [0.88–1.20], which exceed the theoretical value of 1, the expected limit for perovskite structure stability. This can be mainly attributed to the simplifications assumed in the model to estimate the radius of the A–cations, which could fail for very irregularly shaped and anisotropic cations. The first difficulty already arises when trying to set their center of mass, which is often not straightforward.

In this work, and with the aim of facilitating the design of new dicyanamide perovskites as well as other HOIPs containing large A-cations, we propose using the A-cation molecular volume as a means of calculating an effective A-ionic radius. This alternative, and still simple approach is carried out in two steps (Fig. 2, approach 2): first we calculate the "real" volume of the A-site cation using the CrystalExplorer 17 software [26]; second we approximate the obtained volume to that of a sphere to calculate an effective radius for the A-cation. It should also be noted that, in this method, we are using a free and open-access crystallographic software in order to expand the usefulness of the method to the wide scientific community.

To test this method, we focused on dicyanamides $[A][M(dca)_3]$ with M: Mn, as Mn-dicyanamides are the series with more members known so far and whose crystal structures are available in the literature. By analyzing their crystal data we have tried to determine more precisely the volumes of A-cations that can stabilize the perovskite structure and the resulting range of allowed tolerance factors. In a further step, we have selected new A-site cations in order to design new $[A][Mn(dca)_3]$ compounds, which we have prepared and elucidated their crystal structures to confront the experimental results with the predictions resulting from this new approach.

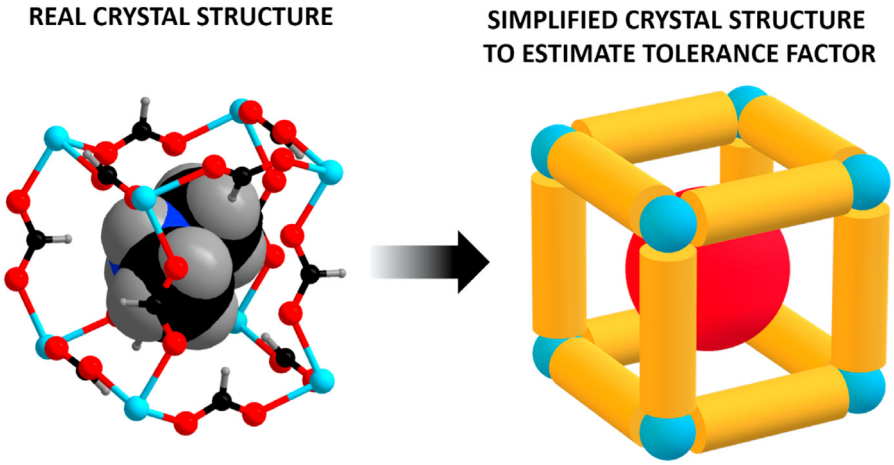

Fig. 1. Comparison of a real hybrid perovskite with the simplified structure used to estimate its extended tolerance factor.

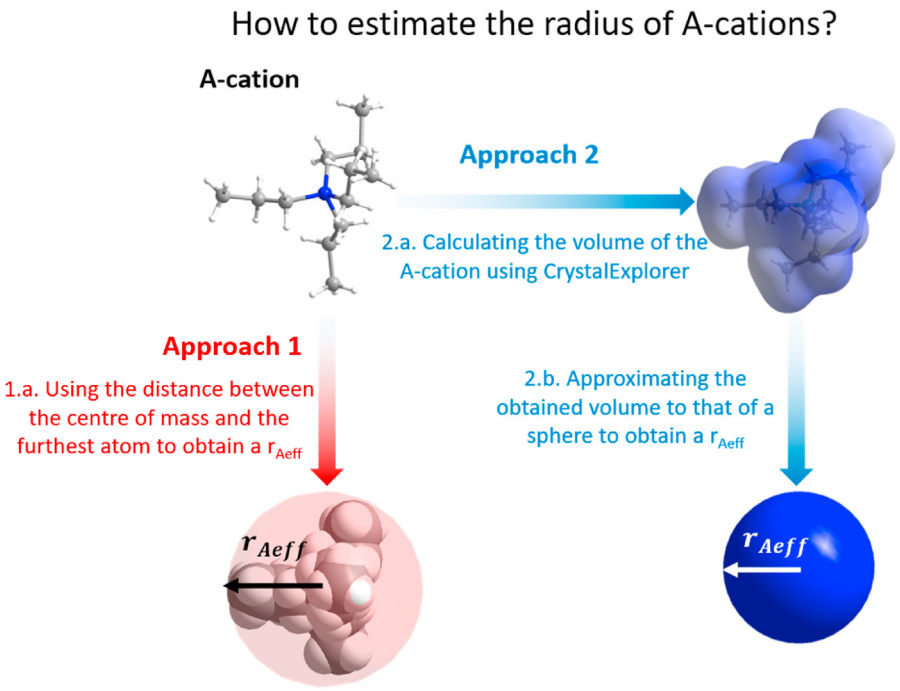

Fig. 2. Two different approaches to estimate the radius of the A-site cations: (1) using the distance between the centre and the furthest atom, as originally proposed by Kieslich et al. (approach 1) and using the here proposed procedure (approach 2). The resulting A-sizes are represented by the pink sphere (approach 1) or the blue sphere (approach 2).

In the course of this study we also became aware of the influence of not only the size but also the shape of the molecular A-cation in the stability of the perovskite. Therefore, we have also explored this second parameter by making use of one of the large number of metrics used to quantify it: the globularity of the A-cation, which is a measure of the degree to which the surface area of a molecule differs from the surface value of a sphere with the same volume [26].

In what follows we present the more relevant aspects and conclusions of these studies.

2. Experimental

2.1. Procedure used to easily calculate the effective volume and radii for A cations and recalculation of extended tolerance factors for [A][Mn(dca)$_3$] compounds

We carried out a literature survey to search for reported crystalline hybrid Mn-dicyanamide compounds with [A][Mn(dca)$_3$] stoichiometry (either with perovskite structure or alternative ones). Until May 2022, we

Table 1
List of A-site cations in reported crystalline hybrid Mn-dicyanamide compounds with general formula [A][Mn(dca)$_3$], and comparison of the A-ionic radius calculated when using approach 1 (Kieslich method) and the here proposed method (approach 2). Abbreviations: Me: methyl group (-CH_3), Et: ethyl group (-CH_2CH_3), Pr: propyl group (-$CH_2CH_2CH_3$), Bu: butyl group (-$CH_2CH_2CH_2CH_3$), Pn: pentyl group (-$CH_2CH_2CH_2CH_2CH_3$), Bn: Benzyl group (-$CH_2C_6H_5$), Ph: phenyl group (C_6H_5) and Cp: cyclopentadienyl (C_5H_5)$^-$.

ID number	A-cation	Perovskite structure	Ionic radius of A-site cations (Å)		Reference
			Approach 1	Approach 2	
1	$[Et_3(CH_2CH_2F)P]^+$	Yes	3.808	3.692	[29]
2	$[Et_3(CH_2CHCH_2)P]^+$	Yes	4.445	3.726	[23]
3	$[Et_3(CH_2OCH_3)P]^+$	Yes	4.62	3.717	[23]
4	$[Et_3(CH_2CH_2Cl)P]^+$	Yes	4.592	3.751	[29]
5	$[Et_3PrP]^+$	Yes	4.911	3.759	[23]
6	$[Pr_3MeN]^+$	Yes	4.651	3.791	[30]
7	$[Et_3BnN]^+$	Yes	5.917	3.916	[18]
8	$[Pr_4N]^+$	Yes	4.628	3.993	[31]
9	$[Pr_3(CH_3CHCH_2OH)N]^+$	Yes	4.745	4.042	[32]
10	$[Pr_3(CH_2CHOHCH_3)N]^+$	Yes	4.72	4.049	[32]
11	$[Bu_3MeN]^+$	Yes	5.868	4.080	[20]
12	$[Ph_3S]^+$	Yes	5.249	4.124	[19]
13	$[Cp^*_2Co]^+$	Yes	3.826	4.404	[33]
14	$[Cp^*_2Fe]^+$	Yes	3.975	4.450	[33]
15	$[Bu_3BnN]^+$	Yes	5.922	4.471	[18]
16	$[Me_3(CH_2CH_2Cl)N]^+$	No	4.38	3.279	[34]
17	$[Me_3(CH_2CH_2Br)N]^+$	No	4.897	3.325	[35]
18	$[Pr_3NH]^+$	No	4.636	3.699	[36]
19	$[EtPh_3P]^+$	No	5.299	4.323	[37]
20	$[Bu_4N]^+$	No	5.802	4.367	[31]
21	$[Ph_4P]^+$	No	5.286	4.504	[38]
22	$[Ph_4As]^+$	No	5.402	4.534	[38]
23	$[Pn_4N]^+$	No	7.107	4.662	[31]

identified 23 compounds which satisfy such criteria and which are summarized in Table 1.

Starting from their available crystallographic data, we used the open access CrystalExplorer software [26] to calculate the A-cation volume enclosed by the "promolecule electron density isosurface" [27], a molecular surface that has been shown to be very similar to other *ab initio* molecular surfaces but easier to calculate [26,27]. This software uses pre-calculated spherical atomic electron density functions and the molecular geometry to generate the promolecule electron density ($\sum_{i\in molecule}^{n}\rho_i(r)$ sums over the atoms belonging to the molecule, where $\rho_i(r)$ is are spherically averaged electron densities for each atom centered on nucleus i) and its isosurfaces [28]. For our study we have used a promolecule isosurface of 0.002 au (~0.013 e Å^{-3}) as it typically contains more than 98% of the electron density associated with that molecule.

After estimating the volume of the polyatomic A-cations by this procedure, we subsequently approximated the obtained volume to that of a sphere to calculate an effective radius for the A-site cation (see Fig. 2, approach 2). Finally, we introduced the as-obtained ionic radii in equation (2) to calculate the extended tolerance factor of the corresponding dicyanamide compounds, by assuming, as in the original approach, that the size of the X-ion remains unchanged and can be estimated in all cases by the same cylinder.

In the case of new A cations, for which no experimental data were available in the literature, we started by designing the A-cation's structure, introduced it in the software Chem3D or Avogadro [39] and allowed the program to optimize bond angles and distances using the computational calculations MM2 force field energy minimization [40,41]. It is worth to note any other software with similar capabilities can also be suitable.

With such input data we subsequently simulated the volume of the A-cation using CrystalExplorer software and we used the as-obtained radii to calculate the theoretical extended tolerance factor for the hypothetical [A][Mn(dca)$_3$] compounds containing such cations.

2.2. Calculation of globularity

The globularity of the A-site cations (G) was calculated using the Crystal Explorer 17 software as G=(S_{sp}/S_m), where S_m is the surface of the A-molecule while S_{sp} is the surface of a sphere of volume equal to that of the A-molecular volume [42]. It is worth noting that, according to this definition, G is 1.0 for a sphere, and progressively less than 1.0 as the molecular surface becomes more structured.

2.3. Synthesis of new dicyanamide compounds

We have synthesized five new [A][Mn(dca)$_3$] compounds, with A: [R$_3$(CH$_2$X)N]$^+$ (R: Et = CH$_3$CH$_2$-, Pr= CH$_3$CH$_2$CH$_2$-, X: Cl or Br) and [Bu$_4$P]$^+$Bu = CH$_3$CH$_2$ CH$_2$CH$_2$-. For this purpose analytical grade Sigma-Aldrich reagents Na(dca) (96%), (CH$_3$CH$_2$)$_3$N (≥99%), (CH$_3$CH$_2$CH$_2$)$_3$N (≥98%), [(CH$_3$CH$_2$CH$_2$CH$_2$)$_4$P]Br (98%), CH$_2$Cl$_2$ (98%), CH$_2$Br$_2$ (≥98.5%) and Mn(NO$_3$)$_2$ 4H$_2$O (≥97%) were used as starting materials.

In the case of the ammonium compounds, their preparation implied, as first step, the synthesis of the halides of the desired A-cations, as [R$_3$(CH$_2$X)N]X ammonium salts are not commercially available.

2.3.1. Synthesis of [R$_3$(CH$_2$X)N]X (R: Et, Pr, X: Cl$^-$, Br$^-$) compounds

The compounds [R$_3$(CH$_2$X)N]X, R: Et, Pr, X: Cl, Br were prepared by mixing R$_3$N in an excess of CH$_2$X$_2$ and stirring at room temperature for 72 h. The resulting white solids were obtained by removing the solvent under reduced pressure at 343K, and the formation of the corresponding phases was corroborated with NMR, see Figs. S1 of Supplementary Information–4 (S.I.).

[Et$_3$(CH$_2$Cl)N]Cl: ^{1}H NMR (300 MHz, CDCl$_3$): δ 5.67 (s, 2H), 3.63 (q, J = 7.2 Hz, 6H), 1.48 (t, J = 7.2 Hz, 9H) ppm.

[Et$_3$(CH$_2$Br)N]Br: ^{1}H NMR (300 MHz, CDCl$_3$): δ 5.53 (s, 2H), 3.66 (q, J = 7.2 Hz, 6H), 1.48 (t, J = 7.2 Hz, 9H) ppm.

[Pr$_3$(CH$_2$Cl)N]Cl: ^{1}H NMR (300 MHz, CDCl$_3$): δ 5.69 (s, 2H), 3.44 (m, J = 8.4 Hz, 6H), 1.83 (m, J = 7.2 Hz, 6H), 1.01 (t, J = 7.2 Hz, 9H) ppm.

[Pr$_3$(CH$_2$Br)N]Br: ^{1}H NMR (300 MHz, CDCl$_3$): δ 5.51 (s, 2H), 3.46 (m, J = 8.4 Hz, 6H), 1.81 (m, J = 7.2 Hz, 6H), 1.00 (t, J = 7.2 Hz, 9H) ppm.

2.3.2. Synthesis of [A][M(dca)$_3$] compounds

[R$_3$(CH$_2$X)N][Mn(dca)$_3$] compounds, with R = Pr, Et and X = Cl, Br, were obtained by slow evaporation of the solution containing the corresponding [R$_3$(CH$_2$X)N]X, Mn(NO$_3$)$_2$·4H$_2$O and Na(dca) reagents in 1:1:3 M proportion. The [Bu$_4$P][Mn(dca)$_3$] compound was also obtained by slow evaporation of the solution containing [Bu$_4$P]Br, Mn(NO$_3$)$_2$ 4H$_2$O and Na(dca) in 1:1:3 M proportion. In all cases, colourless crystals were obtained after a few days at room temperature.

2.4. Nuclear magnetic Resonance

NMR spectra were recorder on a Bruker Advance 300 MHz for 1H equipped with a dual cryoprobe. The solvent used for NMR experiments was CDCl$_3$ (98.5% ACROS Organics).

2.5. Single crystal X-ray diffraction

Single-crystal X-ray diffraction (SCXRD) experiments were carried out at 100 K, 150 K and room temperature. For that purpose, single-crystal diffraction data sets of one crystal were collected at room temperature in a Bruker D8 VENTURE Kappa X-ray diffractometer equipped with a PHOTON III detector and using monochromatic MoKα radiation (λ = 0.71073 Å).

A suitable crystal was chosen and mounted on a MiTeGen MicroMount™ using Paratone® N (Hampton Research). The data integration and reduction were performed using the APEX3 v2019.1–0 (Bruker AXS, 2019) software suite. The integrations of the reflections were performed with SAINT 8.40A and the intensities collected were corrected for Lorentz and polarization effects and for absorption by semi-empirical methods on the basis of symmetry-equivalent data using SADABS 2016/2 of the suite software. The structures were solved by the dual-space algorithm implemented in SHELXT2014/5 program [43] and were refined by least squares method on SHELXL2018/3 [44].

2.6. Powder X-ray diffraction and synchrotron powder X-ray diffraction

Powder X-ray diffraction (PXRD) patterns of the obtained polycrystalline compounds were obtained in a Siemens D-5000 diffractometer with CuK_α radiation at room temperature. Experimental PXRD patterns of the obtained compounds were compared with the simulated PXRD patterns from the crystal structure obtained from single crystal X-ray diffraction (see Fig. S5-7of S.I.).

The results confirm that all the obtained compounds are single phase materials, without secondary phases present. It is worth to note that the apparent unmatching between the simulated and experimental patterns is mainly due to the presence of preferential orientations in the experimental patterns recorded using a Bragg-Brentano geometry; the temperature difference between experimental data (room temperature) and reference data (below room temperature); and probably also, as it is very often the case, disorder processes in the samples at room temperature.

In addition, the Synchrotron powder X-ray diffraction (SPXRD) pattern of [Et$_3$(CH$_2$Br)N] [Mn(dca)$_3$] was recorded at the BM01 beamline of the ESRF Synchrotron (Grenoble, France) using a wavelength of 0.601 Å at room temperature. The wavelength was determined by refining the positions of six individual reflections of a NIST640D silicon standard collected with a Pilatus 2 M detector. The recorded 2D patterns were integrated into a 1D powder profile. For this purpose, the sample was enclosed in a glass capillary (inner diameter φ = 0.5 mm) and in continuous rotation during data collection to improve powder averaging. Rietveld refinement was carried out using the program GSAS-II [45].

3. Results and discussion

3.1. Calculation of effective volume and radii of A cations and tolerance factor for already reported [A][Mn(dca)$_3$] compounds

Following the here proposed methodology, explained in section 2.1., we have calculated the volume and the effective radii of the A-cations of previously reported [A][Mn(dca)$_3$] compounds (see Table 1, calculated A-site ionic radius (approach 2)). With such data we have recalculated their extended tolerance factors, that are plotted against the volume of the A-cation in Fig. 3.

Focusing in the fifteen compounds which exhibit a perovskite structure (corresponding to compounds **1** to **15** in Table 1, and represented as red dots in Fig. 3), the first interesting remark is that when using our method most of their extended tolerance factors nicely range between 0.85 and 0.925 (highlighted with a red shadow in Fig. 3).

Meanwhile, when using the A-site ionic radius obtained following approach 1 (see Table 1), most of the calculated α values are considerable higher, around 1 and above, that is, out of the stability range for perovskites, see Fig. S8 of S.I., where they are compared with the ones obtained using approach 2.

As it can also be seen in Fig. 3, according to our method the volume of the A-cations in the compounds with perovskite structure mainly ranges between 205 and 295 Å^3. Additionally, there are three compounds (**13**, **14** and **15**) with perovskite structure with higher tolerance factors and volumes, α ~0.975 and V~375 A^3, suggesting that probably there is still room to find new members of the family.

As for the lowest α value (~0.85), it corresponds to compound **1** containing the $[Et_3P(CH_2CH_2F)]^+$ A-cation with a volume of 204.62 Å^3. Meanwhile, the highest α value (~0.975) corresponds to the compound **15** containing $[Bu_3(CH_2C_6H_5)N]^+$ as A-cation [18] with a volume of 374.35 Å^3.

To try to learn more about the stability range for the perovskite structure we now pay attention to the other eight dicyanamide compounds [A][Mn(dca)$_3$] with a different structure. For these, we have also estimated the effective volume and the radii of their A-cations and their extended tolerance factors (compounds **16 to 23** in Table 1, represented as black dots in Fig. 3).

In this context, the **16** and **17** compounds with the smallest A-cation, $[Me_3(CH_2CH_2X)N]^+$ (X: Cl or Br) (cation volume 152 Å^3 and the smaller tolerance factors, α ~ 0.8), crystallise in an alternative 2D crystal structure [34,35]. As for the **18** Mn-dicyanamide, with tripropylammonium $[Pr_3NH]^+$ cation, even if its extended tolerance factor seems in principle adequate to stabilize the perovskite structure (A-cation volume = 211.68 Å^3 and α~0.86), the flat molecular geometry of its A-cation is probably an important factor which favours a 2D crystal structure instead of that of the perovskite.

In the opposite extreme of Fig. 3 we find, the Mn-dicyanamide numbered as **23** in Table 1, with the largest A-cation (the tetrapentylammonium $[Pn_4N]^+$ with a volume of 419.97 Å^3), compound which shows a α slightly above 1 (α = 1.004) and crystallizes in a different $LiSbO_3$ structure [31].

Interestingly, Fig. 3 also reveals that compounds 19–22 which show high tolerance factors, but in any case smaller than 1, and close to the value shown by compound 15, can already crystallise in other structures. This is the case of the 21 Mn-dicyanamide with tetraphenylphosphonium [38] $[Ph_4P]^+$ with A-cation volume = 382.60 Å^3 and α = 0.982, and the 20 Mn-dicyanamide with tetrabutylammonium [31] $[Bu_4N]^+$ (A-cation volume = 338.85 Å^3 and α = 0.955), whose reported crystal structures are 2D and triple rutile, respectively.

These findings suggest that, as in the case of inorganic perovskites, close to the tolerance factor limits more than one structural type probably compete and it is difficult to predict which one will form. It seems that in this range there are other factors that affect the stability of the perovskite structure apart from size, among them probably the shape of the A-cations.

To explore the possible role of this shape on the stability of the perovskite structure, we have calculated the globularity of the A-cations present in these dicyanamide compounds.

The obtained results are depicted in Fig. 4, where they are plotted against the tolerance factor of the corresponding [A][Mn(dca)$_3$] compounds. Very interestingly, and as it can be seen there, there is a clear correlation not only between the tolerance factor but also the A-cation globularity and the stability of the perovskite structure. In this context, the compounds with perovskite structure, in general, contain A-cations with globularities higher than 0.75.

On the other hand, there are two groups of non-perovskite compounds: ones whose A-cations present a globularity higher than 0.75, but whose size is too small to stabilize the perovskite structure; and a second group with A-cations of adequate size, but which are strongly anisotropic and show a globularity lower than 0.75.

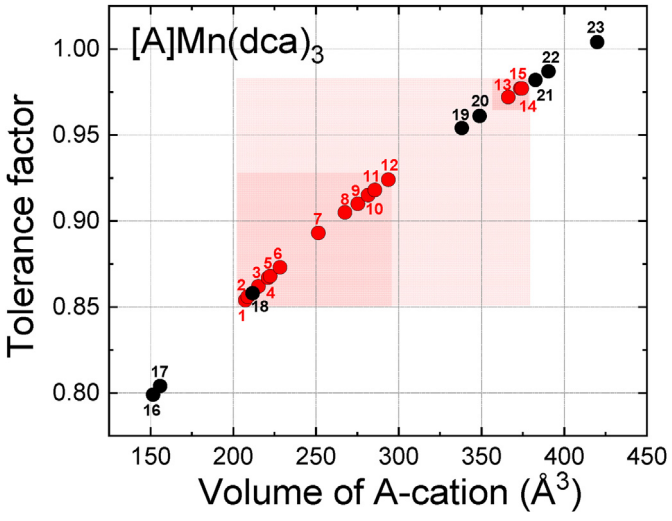

Fig. 3. Tolerance factor versus volume of A-cation for the reported [A][Mn(dca)$_3$] compounds calculated using the here proposed method. Note: red dots: compounds with perovskite structure; black dots: compounds with non-perovskite structure, where the numbers correspond to the compounds listed in Table 1; the dark red shadowed squares indicate regions with existing examples of dicyanamide compounds with perovskite structure, and the lighter red shadow area the region were compounds with such structure might form.

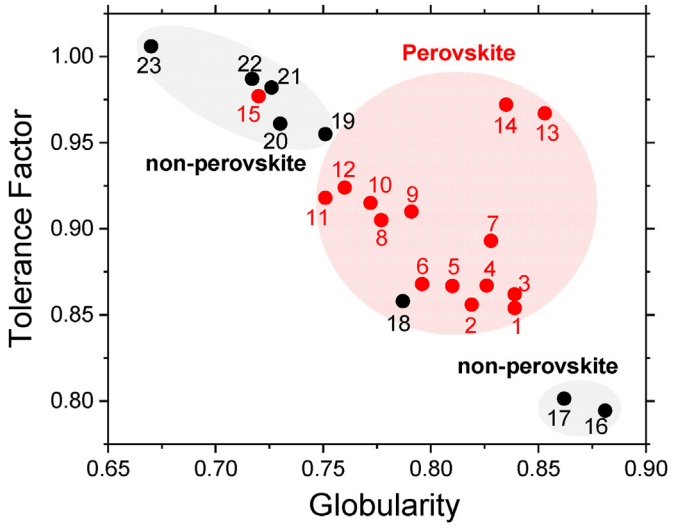

Fig. 4. Plot of tolerance factor versus globularity for the reported [A][Mn(dca)$_3$] compounds, showing the regions were the perovskite structure is (or not) stable.

It is worth to highlight that two compounds, 15 and 18, do not follow this trend. The first one, containing the $[Bu_3BnN]^+$ cation, exhibits a perovskite structure even if the globularity of this A-cation is lower than 0.75. It is worth noting that, as we have previously reported [17] this compound exhibits a very peculiar distortion called cavity sharing, where the long pendant groups of A cation occupy multiple cavities. Therefore, we suggest that this cavity is contributing to stabilize the perovskite structure despite the low globularity value of this A-cation. Meanwhile compound 18, with $[Pr_3NH]^+$, does not exhibit a perovskite structure, even if its tolerance factor and A-cation globularity are, in principle, adequate. It seems that the flat molecular geometry of the tripropylammonium cation, which already is responsible for a globularity value lower than that of related cations (compounds 1 and 2) with similar volume (Figs. 3 and 4), favours the stability of the 2D crystal structure rather than a 3D-perovskite.

In short, from the analysis of the crystallographic data of previously reported $[A][Mn(dca)_3]$ compounds we find that both the size and the shape of the A cations are critical factors to stabilize the perovskite structure. And that, in general, compounds with tolerance factor values ranging between 0.85 and 0.975 and with A-cations with $G > 0.75$ are the ones with more probability to be perovskites.

3.2. New $[A][Mn(dca)_3]$ compounds with specifically designed A-site cations to test the validity of the here proposed approach

In order to obtain new members of this $[A][Mn(dca)_3]$ family and further refine the stability limits of the perovskite structure we have looked for possible A-site cations that can give rise to tolerance factors between ~0.8 and ~1. For that purpose, we have followed the methodology explained in section 2.2. when no structural information is available.

We have also payed attention to their values of globularity, looking for candidates with $G \geq 0.70$.

Finally, we have selected the quaternary ammonium cations $[R_3(CH_2X)N]^+$ (R: CH_3CH_2 (Et), $CH_3CH_2CH_2$ (Pr), X: Cl or Br) sketched in Fig. 5 and indicated in more detail in Table 2, where we include information about their calculated volume, the extended tolerance factor of the resulting hypothetical $[A][Mn(dca)_3]$ compounds and the A-cation globularity.

According to our calculations, the $[Pr_3(CH_2X)N]^+$ (X = Cl, Br) cations (b and c in Table 2) would lead to $[A][Mn(dca)_3]$ dicyanamide compounds with a tolerance factor ~0.9 and A-site globularity ~0.8, so that the perovskite structure would be clearly expected for the resulting compounds (see Fig. 5).

On the other hand, the $[Et_3(CH_2X)N]^+$ (X = Cl, Br) cations (a and b in Table 2) would lead to dicyanamide compounds with a tolerance factor lower than 0.85, in principle, out of the stability range seen so far for the perovskite structure (Fig. 5), even if with an adequate globularity value (high than 0.75).

Additionally, to further explore the stability limits of the perovskite structure we test the compound with the large A-cation $[Bu_4P]^+$, with a volume of 361.02 $Å^3$, and $\alpha = 0.969$, similar to those reported for the largest A-cations with perovskite structure (see Fig. 3), even if with smaller G~0.7 (see Fig. 5).

3.3. Experimental structures for the here prepared new $[A][Mn(dca)_3]$ compounds

We have prepared five new compounds following the synthesis method explained in section 2.2., and we have elucidated their crystal structures. Interestingly, the obtained results show that the three types of cations, namely $[Et_3(CH_2X)N]^+$, $[Pr_3(CH_2X)N]^+$ and $[Bu_4P]^+$, drive into three types of crystal structures, whose main features will be now briefly highlighted:

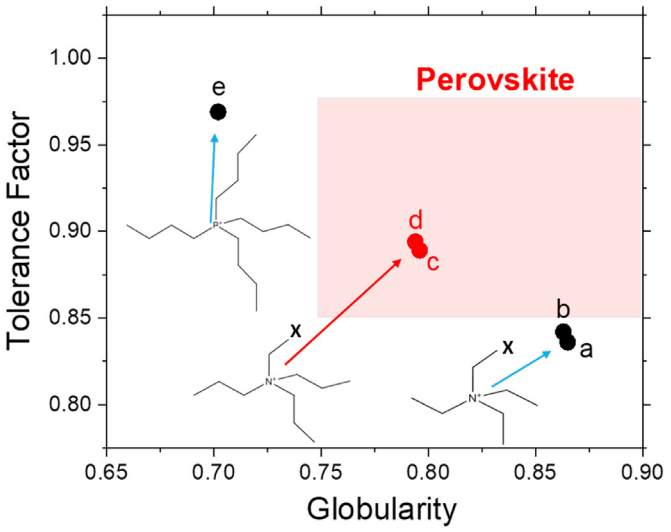

Fig. 5. Tolerance factor versus A-site cation globularity for the here proposed new $[A][M(dca)_3]$ compounds. The circles (red and black, for perovskite and non-perovskite structures, respectively) correspond to the data for A-cations: $[Et_3(CH_2X)N]^+$ (X = Cl, Br), $[Pr_3(CH_2X)N]^+$ (X = Cl, Br) and $[Bu_4P]^+$, a-e in Table 2, whose molecular geometry is also sketched in the graph. The light red shadowed square indicates the region where the perovskite structure is expected to form.

Table 2
List of the A-site cations here designed and synthesized, with their estimated volumes (using the Chem3D software), and globularity values, together with the tolerance factors calculated for the resulting $[A][Mn(dca)_3]$ compounds.

Label	A-cation	Volume ($Å^3$)	α	Globularity
a	$[Et_3(CH_2Cl)N]^+$	187.79	0.836	0.865
b	$[Et_3(CH_2Br)N]^+$	194.23	0.842	0.863
c	$[Pr_3(CH_2Cl)N]^+$	247.97	0.889	0.796
d	$[Pr_3(CH_2Br)N]^+$	254.14	0.894	0.794
e	$[Bu_4P]^+$	361.02	0.969	0.702

3.3.1. Structures of $[Pr_3(CH_2X)N][Mn(dca)_3]$ (X = Cl, Br)

As expected from our calculations, the as-synthesized crystals of $[Pr_3(CH_2Cl)N][Mn(dca)_3]$ and $[Pr_3(CH_2Br)N][Mn(dca)_3]$, compounds **c** and **d**, Table 2, crystallise in a perovskite structure. In both cases they show monoclinic space group $P2_1/n$, and rather similar lattice parameters, even if these are slightly larger in the compound with X = Br, associated to the larger volume of the $[Pr_3(CH_2Br)N]$ cation, namely a = 16.0853(4) Å, b = 16.2405(5), c = 16.4503(5) Å and β = 97.648(1) for X = Cl and a = 16.1458(11) Å b = 16.2630(13), c = 16.4926(13) (5) Å and β = 96.469(3) at 100 K, for X = Br (see more details on Table S1 of S.I.).

In both compounds, each Mn^{2+} is octahedrally coordinated to its neighbouring Mn^{2+} cations through six $\mu_{1,5}$-[dca]-bridges forming the 3D $[Mn(dca)_3]^-$ framework with the $[Pr_3(CH_2X)N]^+$ cations sitting in the pseudocuboctahedra cavities, as expected for a perovskite structure (Fig. 6).

Interestingly, in both $[Pr_3(CH_2X)N][Mn(dca)_3]$ (X = Cl or Br) compounds the $\mu_{1,5}$-[dca]-bridges show both syn–anti and anti–coordination modes, depending on the crystallographic direction. Additionally, the presence of these dca ligands allow for both conventional (reported on pure inorganic perovskites) or unconventional (exclusive of hybrid perovskites) [46] $[MnN_6]$ octahedral tilts, and $[MnN_6]$ columnar shifts [47], provoking large distortions of the 3D-perovskite framework.

In particular, the $[MnN_6]$ octahedral tilt pattern shows one in-phase and two out-of-phase tilts with the Glazer notation (a^- b^+ c^-). As for the columnar shifts, they are active along the three main axis, with a shifted out-of-phase relative to their immediate neighbours, and are specially large along c-axis (see Fig. S9 of S.I.).

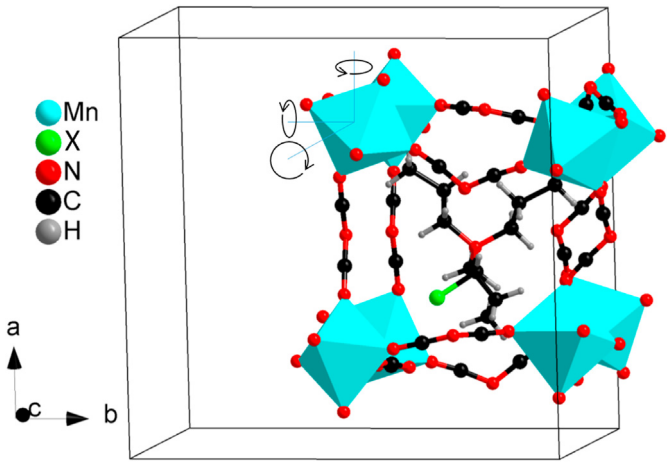

Fig. 6. Detail of the crystal structure of $[Pr_3(CH_2X)N][Mn(dca)_3]$ (X = Cl or Br) at 100 K, showing a highly distorted $[Mn(dca)_3]^-$ framework and a cooperative octahedral tilting along the three main axis.

Table 3
Comparison of the volume of A-cations obtained by geometrical optimization of the cations and the experimental values calculated from crystal structure data following the approach 1 and the here proposed approach 2 indicated in section 2.1.

A-cation	Cation volume from geometrical optimization (Å^3)	Cation volume, from crystallographic data (Å^3), approach 1	Cation volume, from crystallographic data (Å^3), approach 2
$[Pr_3(CH_2Cl)N]^+$	247.97	356.8	245.23
$[Pr_3(CH_2Br)N]^+$	254.14	381.7	251.07

To further test the validity of the here proposed approximation, that very nicely predicts the formation of the perovskite structure, we have also compared the volume of the A-cations obtained from the geometrical optimization carried out with the software Chem3D with those obtained from experimental data applying approach 1 and the here proposed approach 2. As shown in Table 3 there is a very good agreement between the values obtained by the geometrical optimization and the volume calculated using approach 2, explained in section 2.1.

Meanwhile the volume calculated for the A-cations using approach 1 turns to be again higher (see Table 3) probably because when using such approach with irregularly shaped A-cations, empty void spaces are included as if they were part of the cation, which is not really the case, resulting in an overestimation of their size (see sketch in Fig. 2).

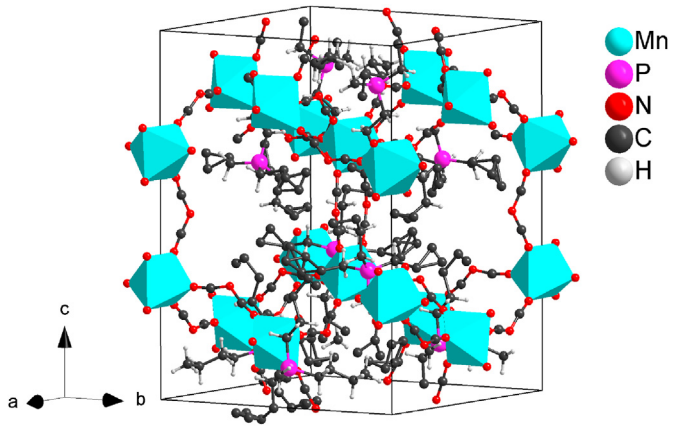

Fig. 8. Crystal structure of $[Bu_4P][Mn(dca)_3]$ at room temperature.

On the other hand, the good matching between the first two in turn implies that the estimated volume of the A-cation using a simple software for molecular geometry optimization, that can subsequently be used to calculate the tolerance factor, can be a powerful and very simple tool to predict the formation (or not) of new $[A][Mn(dca)_3]$ dicyanamide perovskites. This is especially useful when A-cations are complex and difficult to prepare.

3.3.2. *Structures of $[Et_3(CH_2X)N][Mn(dca)_3]$ (X = Cl, Br)*

$[Et_3(CH_2Cl)N][Mn(dca)_3]$, compound a in Table 2, crystallizes in the monoclinic *C2/m* space group with a = 14.9722(3) Å, b = 17.2255(3) Å, c = 7.4663(2) Å and β = 102.724(1) (see more details in Table S2 of S.I.). It contains one atom of oxygen inside its crystal assembly, suggesting that the compound is monohydrated.

Interestingly, at difference with the compounds described in the previous section 3.3.(a), this compound does not show a perovskite structure, but a layered structure similar to the previously reported for the $[Me_3(CH_2CH_2X)N][M(dca)_3]$ compounds with M = Mn and Cd [34, 35]. It basically consists of a 2D $[Mn(dca)_3]^-$ anionic scaffold complemented by the $[Et_3(CH_2Cl)N]^+$ cations acting as counterions and one water molecule per formula (see Fig. 7). Within the 2D layered

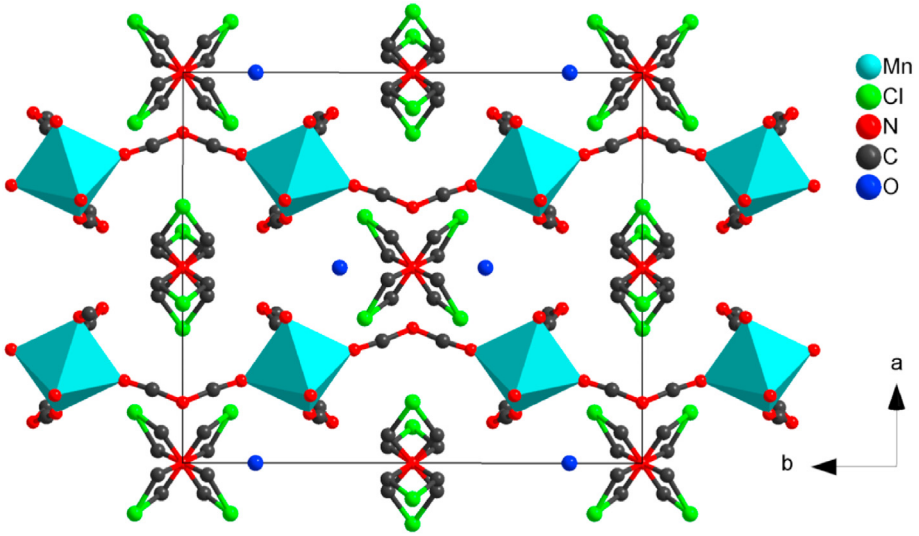

Fig. 7. Crystal structure of $[Et_3(CH_2Cl)N][Mn(dca)_3]\cdot H_2O$ at 150 K.

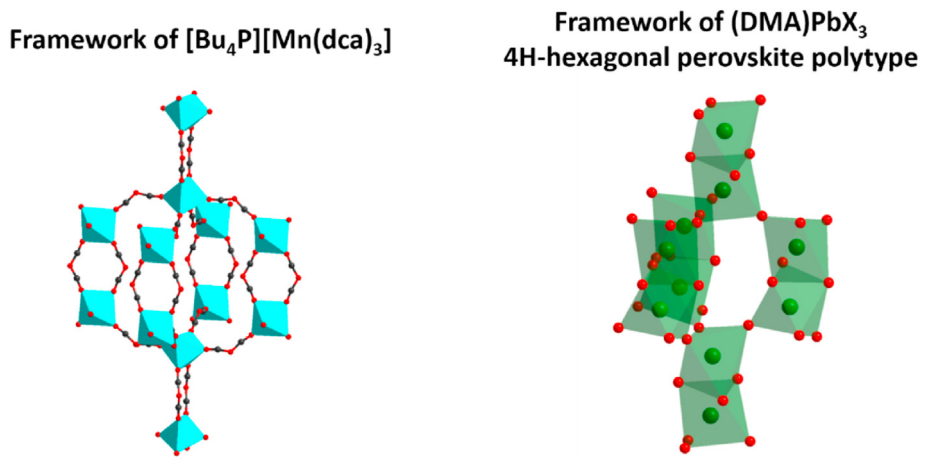

Fig. 9. Details of the crystal structure of $[Bu_4P][Mn(dca)_3]$ showing the arrangement of the framework (on the left), compared to the 4H-hexagonal perovskite polytype of $(DMA)PbX_3$, where DMA is dimethylammonium cation and X is chloride or bromide anions (on the right).

$[Mn(dca)_3]^-$ network structure, each Mn^{2+} cation is octahedrally coordinated by six N atoms from six bridging dca ligands, and the neighbouring metal cations are linked to four Mn^{2+} cations in two different ways: by double dca-bridges to two Mn^{2+} cations (along the c-axis) and by single dca-bridges to other two Mn^{2+} cations (along the b-axis) (see details in Fig. S10 of S.I.).

Such 2D $Mn(dca)_3^-$ layers are stacking along the a-axis and the spaces between adjacent layers are filled with $Et_3(CH_2Cl)N^+$ cations and water molecules. Strong disorder is observed in the A-site cations, with the C and Cl atoms located at 8 and 4 different crystallographic sites, respectively, while the N-atoms sit in a single crystallographic site.

The structure of $[Et_3(CH_2Br)N][Mn(dca)_3]$, compound **b** in Table 2—for which we could not obtain single crystals— could be elucidated by Synchrotron X-ray powder diffraction. According to the as-obtained results (Fig. S11 of S.I.), it is similar to that shown by the X = Cl compound, with slighltly larger cell parameters —as expected in view of the larger volume of the $[Et_3(CH_2Br)N]^+$ cation—, namely a = 15.2521(8) Å, b = 17.2552(3) Å, c = 7.5481(3) Å and β = 100.867(2) at room temperature (see more details in Table S3 of S.I.).

Therefore, as none of the $[Et_3(CH_2X)N][Mn(dca)_3]$ (X = Cl, Br) compounds exhibit the perovskite structure, we deduce that the size of the used A-cation and thus the tolerance factor of the obtained compounds are not large enough to stabilize it, even if the globularity of the $[Et_3(CH_2X)N]^+$ cation would be adequate, G > 0.75.

This is also an interesting result that helps to better defining the lower limit of the tolerance factor and the volume of the A-cations to stabilize the perovskite structure and confirms the power of the predictions. Thus, we establish that the minimum size of A-site cations in $[A][Mn(dca)_3]$ compounds to obtain a perovskite structure should be in the range of [195−205] $Å^3$ and the lower limit of the tolerance factor should be in the range of [0.84–0.85].

3.3.3. *Structure of $[Bu_4P][Mn(dca)_3]$*

$[Bu_4P][Mn(dca)_3]$, compound **e** in Table 2, crystallises in the orthorhombic space group $P2_12_12$ (non-centrosymmetric) with lattice parameters a = 16.268(6) Å, b = 16.323(6) Å and c = 21.550(7) Å at 295 K (see more details on Table S4 of S.I. and Fig. 8). This compound does not show either the perovskite structure, but a framework in which each octahedrally coordinated Mn^{2+} is connected to five neighbouring Mn^{2+} cations through $\mu_{1,5}$-[dca]-bridges: to four of them through simple dca bridges and to the fifth one through two dca ligands resulting in an edge sharing configuration (see Fig. S12 of S.I.).

As shown in more detail in Fig. 9, the arrangement of this framework can be described as formed by $[Mn_2(dca)_{10}]^{6-}$ dimers, which are comprised of two edge-sharing octahedra (connected by two bridging dca anions) and each dimer is linked to other eight neighbouring dimers by corner-sharing octahedra. This arrangement has clear reminiscences to that shown by some oxide and hybrid hexagonal perovskites. In particular, it is very similar to the structure shown by the $(DMA)PbX_3$ compounds (with DMA = dimethylammonium cation and X = Cl, Br), that exhibit a 4H-hexagonal perovskite polytype [48] (see Fig. 8). This is a very common crystal structure observed in purely inorganic ABX_3 compounds when the A-cation is too large to be located in the cuboctahedra cavity of the perovskite structure.

In fact, the here presented framework creates a rather large cavity delimited by ten $[MnN_6]$ octahedra, in contrast to the eight $[MnN_6]$ present in a perovskite structure, where the very bulky $[Bu_4P]$ cations (which in addition show partially disorder in the C-atoms in three of the four butyl groups) can be accommodated.

It should also be pointed out that the relatively lower globularity value of this cation (G~ 0.70) is also another factor playing against the stabilisation of this compound in the perovskite structure.

4. Conclusions

We propose an alternative method to calculate the effective volume and radii of A-cations, whether previous crystallographic data are available or not, that helps predicting the stability of perovskite structures through the tolerance factor approach. The reported methodology, which is carried out in an easy way, is especially useful when large and irregular A-cations are present, and avoids, for example the difficulty to estimate their center of mass or overestimation of their size.

Despite the simplicity of the method, we demonstrate that it behaves reasonably well to predict, in a first approach, the stability of $[A][Mn(dca)_3]$ dicyanamide perovskites. In this context, we have established the lower and upper tolerance factor and A-site volume limits for such perovskite dicyanamides more precisely, which may help in the search for new members of this emerging family of (multi)functional multi(stimuli)-responsive materials. In particular, we have observed that in most $[A][Mn(dca)_3]$ perovskites the A-cation volume lies between 200 and 300 $Å^3$ ($0.85 < \alpha < 0.925$), and we have experimentally obtained two new members of the family falling in this range. In addition there is probably still room to find new members of the family for A-cations with a size between 300 and 400 $Å^3$ ($0.925 < \alpha < 1$).

In addition, we show that the shape of the A-cation plays also a role in the stabilisation of the perovskite structure. In that context, we establish a minimum globularity value G > 0.75 that favors the formation of the

structure, provided that the size of the A-cation, and thus the tolerance factor is also adequate.

In any case, there could be could be other factors involved that have not been considered in this simple approach, among which the liberation of pendant groups of the A cations could also be important in some cases.

Finally, it is worth noting that the here proposed methodology, which we have initially developed to facilitate the design of new dicyanamide perovskites, is not only valid for this particular family but very useful for any other hybrid perovskites and related materials.

For example, most recently Burger et al. [49] have reported new and very interesting perovskite-like AB_2X_6 compounds based on a $[BX_3]^-$ ReO_3-type host network ($[Mn(C_2N_3)_3]^-$), in which the divalent A^{2+} cations ($[Pr_3N(CH_2)_nNPr_3]^{2+}$ with n = 4 and 5) with separated charge centers bridge adjacent A-site cavities. To test the validity of the here proposed procedure beyond "conventional" perovskites, we have estimated the volume of these two divalent organic A-cations using the CrystalExplorer software. We then divided the obtained volumes by two, as each of the divalent cation occupies two A-sites, to subsequently approach them to that of a sphere to calculate an effective radius, according to the here explained approach 2. Very interestingly, the as-estimated tolerance factor and globularity values for these compounds turn to be: $\alpha = 0.885$, $G = 0.80$ when A^{2+}: $[Pr_3N(CH_2)_4NPr_3]^{2+}$; and $\alpha = 0.893$, $G = 0.79$ when A^{2+}: $[Pr_3N(CH_2)_5NPr_3]^{2+}$. That is both values nicely fit within the range that we have defined as stable for the perovskite structure.

CRediT authorship contribution statement

Javier García-Ben: Investigation, Methodology, Validation. **Alberto García-Fernández:** Investigation, Writing – review & editing. **Pedro Dafonte-Rodríguez:** Investigation. **Ignacio Delgado-Ferreiro:** Investigation. **Ute B. Cappel:** Writing – review & editing. **Socorro Castro-García:** Writing – review & editing. **Manuel Sánchez-Andújar:** Conceptualization, Supervision, Writing – original draft. **Juan Manuel Bermúdez-García:** Methodology, Writing – review & editing. **María Antonia Señarís-Rodríguez:** Conceptualization, Writing – original draft, Writing – review & editing.

Declaration of competing interest

The authors declare that they have no known competing financial interests or personal relationships that could have appeared to influence the work reported in this paper.

Data availability

Data will be made available on request.

Acknowledgements

M.A. S-R, who had the privilege and the pleasure of being a Ph.D student of Professor Alario, acknowledge the inspiration and imprint received from Miguel. His enormous and pioneering scientific capabilities and competences, together with his generous and contagious vital enthusiasm, have been a reference for her and her group in Galicia all along these years.

As for financial support, the authors thank Ministerio de Economía y Competitividad MINECO and EU-FEDER (projects MAT2017-86453-R and PDC2021-121076-I00), and Xunta de Galicia for the collaboration agreement "Development of research strategic actions Universidade da Coruña I + D + i 2021–2022: CICA-Disrupting Projects 2021SEM-A3 (NanoCool). J.G.-B. and J.M.B.-G. acknowledge Xunta de Galicia for Predoctoral and Postdoctoral Fellowships, respectively. I.D.-F thanks Ministerio de Universidades for a FPU Predoctoral Fellowship. A. G.-F. and U.B.C thank the Carl Tryggers foundation and the Göran Gustafsson foundation for financial support.

Appendix A. Supplementary data

Supplementary data to this article can be found online at https://doi.org/10.1016/j.jssc.2022.123635.

References

[1] F.T. Szczypiński, S. Bennett, K.E. Jelfs, Can we predict materials that can be synthesised? Chem. Sci. 12 (2021) 830–840, https://doi.org/10.1039/d0sc04321d.
[2] C. Shi, C.H. Yu, W. Zhang, Predicting and screening dielectric transitions in a series of hybrid organic-inorganic double perovskites via an extended tolerance factor Approach, Angew. Chemie - Int. Ed. 55 (2016) 5798–5802, https://doi.org/10.1002/ANIE.201602028.
[3] V.M. Goldschmidt, Die gesetze der Krystallochemie, Naturwissenschaften 14 (1926) 477–485, https://doi.org/10.1007/BF01507527.
[4] A.M. Glazer, The classification of tilted octahedra in perovskites, Acta Crystallogr. Sect. B Struct. Crystallogr. Cryst. Chem. 28 (1972) 3384–3392, https://doi.org/10.1107/S0567740872007976.
[5] G. Kieslich, S. Sun, A.K. Cheetham, Solid-state principles applied to organic-inorganic perovskites: new tricks for an old dog, Chem. Sci. 5 (2014) 4712–4715, https://doi.org/10.1039/C4SC02211D.
[6] G. Kieslich, S. Sun, A.K. Cheetham, An extended Tolerance Factor approach for organic-inorganic perovskites, Chem. Sci. 6 (2015) 3430–3433, https://doi.org/10.1039/C5SC00961H.
[7] S. Burger, M.G. Ehrenreich, G. Kieslich, Tolerance factors of hybrid organic-inorganic perovskites: recent improvements and current state of research, J. Mater. Chem. A. 6 (2018) 21785–21793, https://doi.org/10.1039/C8TA05794J.
[8] W. Li, A. Stroppa, Z. Wang, S. Gao, Hybrid Organic-Inorganic Perovskites, Wiley, 2020, https://doi.org/10.1002/9783527344338.
[9] W. Li, Z. Wang, F. Deschler, S. Gao, R.H. Friend, A.K. Cheetham, Chemically diverse and multifunctional hybrid organic-inorganic perovskites, Nat. Rev. Mater. 2 (2017), 16099, https://doi.org/10.1038/natrevmats.2016.99.
[10] H.L.B. Boström, A.L. Goodwin, Hybrid perovskites, metal-organic frameworks, and beyond: unconventional degrees of freedom in molecular frameworks, Acc. Chem. Res. 54 (2021) 1288–1297, https://doi.org/10.1021/acs.accounts.0c00797.
[11] A. Kojima, K. Teshima, Y. Shirai, T. Miyasaka, Organometal halide perovskites as visible-light sensitizers for photovoltaic cells, J. Am. Chem. Soc. 131 (2009) 6050–6051, https://doi.org/10.1021/ja809598r.
[12] T.J. Jacobsson, A. Hultqvist, A. García-Fernández, A. Anand, A. Al-Ashouri, A. Hagfeldt, A. Crovetto, A. Abate, A.G. Ricciardulli, A. Vijayan, A. Kulkarni, A.Y. Anderson, B.P. Darwich, B. Yang, B.L. Coles, C.A.R. Perini, C. Rehermann, D. Ramirez, D. Fairen-Jimenez, D. Di Girolamo, D. Jia, E. Avila, E.J. Juarez-Perez, F. Baumann, F. Mathies, G.S.A. González, G. Boschloo, G. Nasti, G. Paramasivam, G. Martínez-Denegri, H. Näsström, H. Michaels, H. Köbler, H. Wu, I. Benesperi, M.I. Dar, I. Bayrak Pehlivan, I.E. Gould, J.N. Vagott, J. Dagar, J. Kettle, J. Yang, J. Li, J.A. Smith, J. Pascual, J.J. Jerónimo-Rendón, J.F. Montoya, J.P. Correa-Baena, J. Qiu, J. Wang, K. Sveinbjörnsson, K. Hirselandt, K. Dey, K. Frohna, L. Mathies, L.A. Castriotta, M.H. Aldamasy, M. Vasquez-Montoya, M.A. Ruiz-Preciado, M.A. Flatken, M.V. Khenkin, M. Grischek, M. Kedia, M. Saliba, M. Anaya, M. Veldhoen, N. Arora, O. Shargaieva, O. Maus, O.S. Game, O. Yudilevich, P. Fassl, Q. Zhou, R. Betancur, R. Munir, R. Patidar, S.D. Stranks, S. Alam, S. Kar, T. Unold, T. Abzieher, T. Edvinsson, T.W. David, U.W. Paetzold, W. Zia, W. Fu, W. Zuo, V.R.F. Schröder, W. Tress, X. Zhang, Y.H. Chiang, Z. Iqbal, Z. Xie, E. Unger, An open-access database and analysis tool for perovskite solar cells based on the FAIR data principles, Nat. Energy 7 (2022) 107–115, https://doi.org/10.1038/s41560-021-00941-3.
[13] H.L.B. Boström, M.S. Senn, A.L. Goodwin, Recipes for improper ferroelectricity in molecular perovskites, Nat. Commun. 9 (2018) 2380, https://doi.org/10.1038/s41467-018-04764-x.
[14] J.M. Bermúdez-García, M. Sánchez-Andújar, S. Castro-García, J. López-Beceiro, R. Artiaga, M.A. Señarís-Rodríguez, Giant barocaloric effect in the ferroic organic-inorganic hybrid [TPrA][Mn(dca)3] perovskite under easily accessible pressures, Nat. Commun. 8 (2017), 15715, https://doi.org/10.1038/ncomms15715.
[15] J.M. Bermúdez-García, M. Sánchez-Andújar, M.A. Señarís-Rodríguez, A new playground for organic-inorganic hybrids: barocaloric materials for pressure-induced solid-state cooling, J. Phys. Chem. Lett. 8 (2017) 4419–4423, https://doi.org/10.1021/acs.jpclett.7b01845.
[16] J. Salgado-Beceiro, A. Nonato, R.X. Silva, A. García-Fernández, M. Sánchez-Andújar, S. Castro-García, E. Stern-Taulats, M.A. Señarís-Rodríguez, X. Moya, J.M. Bermúdez-García, Near-room-temperature reversible giant barocaloric effects in [(CH3)4N]Mn[N3]3 hybrid perovskite, Mater, Adv 1 (2020) 3167–3170, https://doi.org/10.1039/D0MA00652A.
[17] J. García-Ben, L.N. McHugh, T.D. Bennett, J.M. Bermúdez-García, Dicyanamide-perovskites at the edge of dense hybrid organic-inorganic materials, Coord. Chem. Rev. 455 (2022), https://doi.org/10.1016/j.ccr.2021.214337.
[18] M.-L. Tong, J. Ru, Y.-M. Wu, X.-M. Chen, H.-C. Chang, K. Mochizuki, S. Kitagawa, Cation-templated construction of three-dimensional α-Po cubic-type [M(dca)3]-networks. Syntheses, structures and magnetic properties of A[M(dca)3] (dca = dicyanamide; for A = benzyltributylammonium, M = Mn2+, Co2+; for A = benzyltriethylammonium, M = Mn2, New J. Chem. 27 (2003) 779–782, https://doi.org/10.1039/b300760j.
[19] J.A. Schlueter, J.L. Manson, K.A. Hyzer, U. Geiser, Spin canting in the 3D anionic dicyanamide structure (SPh 3)Mn(dca) 3 (Ph = phenyl, dca = dicyanamide), Inorg. Chem. 43 (2004) 4100–4102, https://doi.org/10.1021/ic035398p.

[20] M. Mączka, A. Gągor, M. Ptak, D. Stefańska, L. Macalik, A. Pikul, A. Sieradzki, Structural, phonon, magnetic and optical properties of novel perovskite-like frameworks of TriBuMe[M(dca) 3] (TriBuMe = tributylmethylammonium; dca = dicyanamide; M = Mn 2+ , Fe 2+ , Co 2+ , Ni 2+), Dalton Trans. 48 (2019) 13006–13016, https://doi.org/10.1039/C9DT02924A.
[21] Z.B. Liu, L. He, P.P. Shi, Q. Ye, D.W. Fu, A three-dimensional molecular perovskite ferroelastic with two-step switching of quadratic nonlinear optical properties tuned by molecular chiral design, J. Phys. Chem. Lett. 11 (2020) 7960–7965, https://doi.org/10.1021/acs.jpclett.0c02235.
[22] J.M. Bermúdez-García, M. Sánchez-Andújar, S. Yáñez-Vilar, S. Castro-García, R. Artiaga, J. López-Beceiro, L. Botana, Á. Alegría, M.A. Señarís-Rodríguez, Role of temperature and pressure on the multisensitive multiferroic dicyanamide framework [TPrA][Mn(dca) 3] with perovskite-like structure, Inorg. Chem. 54 (2015) 11680–11687, https://doi.org/10.1021/acs.inorgchem.5b01652.
[23] F.J. Geng, L. Zhou, P.P. Shi, X.L. Wang, X. Zheng, Y. Zhang, D.W. Fu, Q. Ye, Perovskite-type organic-inorganic hybrid NLO switches tuned by guest cations, J. Mater. Chem. C 5 (2017) 1529–1536, https://doi.org/10.1039/C6TC05105G.
[24] J.M. Bermúdez-García, S. Yáñez-Vilar, A. García-Fernández, M. Sánchez-Andújar, S. Castro-García, J. López-Beceiro, R. Artiaga, M. Dilshad, X. Moya, M.A. Señarís-Rodríguez, Giant barocaloric tunability in [(CH3CH2CH2)4N]Cd[N(CN)2]3 hybrid perovskite, J. Mater. Chem. C 6 (2018) 9867–9874, https://doi.org/10.1039/c7tc03136j.
[25] M.M. Zhao, L. Zhou, P.P. Shi, X. Zheng, X.G. Chen, J.X. Gao, F.J. Geng, Q. Ye, D.W. Fu, Halogen substitution effects on optical and electrical properties in 3D molecular perovskites, Chem. Commun. 54 (2018) 13275–13278, https://doi.org/10.1039/c8cc07052k.
[26] P.R. Spackman, M.J. Turner, J.J. McKinnon, S.K. Wolff, D.J. Grimwood, D. Jayatilaka, M.A. Spackman, CrystalExplorer: a program for Hirshfeld surface analysis, visualization and quantitative analysis of molecular crystals, J. Appl. Crystallogr. 54 (2021) 1006–1011, https://doi.org/10.1107/S1600576721002910.
[27] A.S. Mitchell, M.A. Spackman, Molecular surfaces from the promolecule: a comparison with Hartree-Fockab initio electron density surfaces, J. Comput. Chem. 21 (2000) 933–942, https://doi.org/10.1002/1096-987X(200008)21:11<933::AID-JCC3>3.0.CO;2-F.
[28] M.A. Spackman, P.R. Spackman, S.P. Thomas, 13 beyond Hirshfeld surface analysis: interaction energies, energy frameworks and lattice energies with CrystalExplorer, Complement. Bond. Anal. (2021) 329–352, https://doi.org/10.1515/9783110660074-013.
[29] M. Zhao, L. Zhou, P. Shi, X. Zheng, X. Chen, J. Gao, L. He, Q. Ye, C. Liu, D. Fu, 3D organic-norganic perovskite ferroelastic materials with two ferroelastic phases: [Et3P(CH2)2F][Mn(dca)3] and [Et3P(CH2)2Cl][Mn(dca)3], Chem. Eur J. 25 (2019) 6447–6454, https://doi.org/10.1002/chem.201900771.
[30] S. Burger, S. Grover, K.T. Butler, H.L.B. Boström, R. Grau-Crespo, G. Kieslich, Tilt and shift polymorphism in molecular perovskites, Mater. Horiz. 8 (2021) 2444–2450, https://doi.org/10.1039/d1mh00578b.
[31] J. a Schlueter, J.L. Manson, U. Geiser, Structural and magnetic diversity in tetraalkylammonium salts of anionic M[N(CN)2]3(-) (M = Mn and Ni) three-dimensional coordination polymers, Inorg. Chem. 44 (2005) 3194–3202, https://doi.org/10.1021/ic0484598.
[32] Z. Liu, L. He, P. Shi, Q. Ye, A three-dimensional molecular perovskite ferroelastic with two- step switching of quadratic nonlinear optical properties tuned by molecular chiral design. https://doi.org/10.1021/acs.jpclett.0c02235, 2020.
[33] P.M. Van Der Werff, E. Martínez-Ferrero, S.R. Batten, P. Jensen, C. Ruiz-Pérez, M. Almeida, J.C. Waerenborgh, J.D. Cashion, B. Moubaraki, J.R. Galán-Mascarós, J.M. Martínez-Agudo, E. Coronado, K.S. Murray, Hybrid materials containing organometallic cations and 3-D anionic metal dicyanamide networks of type [Cp*2M][M'(dca)3], Dalton Trans. (2005) 285–290, https://doi.org/10.1039/B415275A.
[34] S.S. Wang, R.K. Huang, X.X. Chen, W.J. Xu, W.X. Zhang, X.M. Chen, Temperature-induced structural phase transitions in two new postperovskite coordination polymers, Cryst. Growth Des. 19 (2019) 1111–1117, https://doi.org/10.1021/acs.cgd.8b01615.
[35] S.S. Wang, X.X. Chen, B. Huang, R.K. Huang, W.X. Zhang, X.M. Chen, Unique freezing dynamics of flexible guest cations in the first molecular postperovskite ferroelectric: (C5H13NBr)[Mn(N(CN)2)3], CCS Chem 1 (2019) 448–454, https://doi.org/10.31635/CCSCHEM.019.20190012.
[36] Y. Huang, X. Yu, Z. Rong, Y. Ai, K. Qian, J. Yang, Ferromagnetic interactions in a dicyanamide-bridged multinuclear metal-organic framework [Pr3NH]+ [Mn(dca)3]- ·H 2 O, Z. Naturforsch. B Chem. Sci. 74 (2019) 485–489, https://doi.org/10.1515/znb-2019-0015.
[37] P.M. van der Werff, S.R. Batten, P. Jensen, B. Moubaraki, K.S. Murray, J.D. Cashion, Structure and magnetism of 3D anionic metal dicyanamide (MePh 3 P)[M(dca) 3] (M = Fe, Co, Ni) and (EtPh 3 P)[M(dca) 3] (M = Mn, Co, Ni) networks, cryst, Growth Des 4 (2004) 503–508, https://doi.org/10.1021/cg034258n.
[38] J.W. Raebiger, J.L. Manson, R.D. Sommer, U. Geiser, A.L. Rheingold, J.S. Miller, 1-D and 2-D homoleptic dicyanamide structures, [Ph 4 P] 2 {Co II [N(CN) 2] 4 } and [Ph 4 P]{M[N(CN) 2] 3 } (M = Mn, Co), inorg, Chem 40 (2001) 2578–2581, https://doi.org/10.1021/ic001379t.
[39] M.D. Hanwell, D.E. Curtis, D.C. Lonie, T. Vandermeersch, E. Zurek, G.R. Hutchison, Avogadro: an advanced semantic chemical editor, visualization, and analysis platform, J. Cheminf. 4 (2012) 17, https://doi.org/10.1186/1758-2946-4-17.
[40] N.L. Allinger, Y.H. Yuh, J.H. Lii, Molecular mechanics. The MM3 force field for hydrocarbons. 1, J. Am. Chem. Soc. 111 (1989) 8551–8566, https://doi.org/10.1021/ja00205a001.
[41] N.L. Allinger, Conformational analysis. 130. MM2. A hydrocarbon force field utilizing V1 and V2 torsional terms, J. Am. Chem. Soc. 99 (1977) 8127–8134, https://doi.org/10.1021/ja00467a001.
[42] J.J. McKinnon, A.S. Mitchell, M.A. Spackman, Hirshfeld surfaces: a new tool for visualising and exploring molecular crystals, Chem. Eur J. 4 (1998) 2136–2141, https://doi.org/10.1002/(SICI)1521-3765(19981102)4:11<2136::AID-CHEM2136>3.0.CO;2-G.
[43] G.M. Sheldrick, IUCr, *SHELXT* - integrated space-group and crystal-structure determination, Acta Crystallogr. Sect. A Found. Adv. 71 (2015) 3–8, https://doi.org/10.1107/S2053273314026370.
[44] G.M. Sheldrick, Crystal structure refinement with SHELXL, Acta Crystallogr. Sect. C Struct. Chem. 71 (2015) 3–8, https://doi.org/10.1107/S2053229614024218.
[45] B.H. Toby, R.B. Von Dreele, GSAS-II: the genesis of a modern open-source all purpose crystallography software package, J. Appl. Crystallogr. 46 (2013) 544–549, https://doi.org/10.1107/S0021889813003531.
[46] S.G. Duyker, J.A. Hill, C.J. Howard, A.L. Goodwin, Guest-activated forbidden tilts in a molecular perovskite analogue, J. Am. Chem. Soc. 138 (2016) 11121–11123, https://doi.org/10.1021/jacs.6b06785.
[47] I.E. Collings, J.A. Hill, A.B. Cairns, R.I. Cooper, A.L. Thompson, J.E. Parker, C.C. Tang, A.L. Goodwin, Compositional dependence of anomalous thermal expansion in perovskite-like ABX 3 formates, Dalton Trans. 45 (2016) 4169–4178, https://doi.org/10.1039/C5DT03263F.
[48] A. García-Fernández, E.J. Juarez-Perez, J.M. Bermúdez-García, A.L. Llamas-Saiz, R. Artiaga, J.J. López-Beceiro, M.A. Señarís-Rodríguez, M. Sánchez-Andújar, S. Castro-García, Hybrid lead halide [(CH3)2NH2]PbX3 (X = Cl- and Br) hexagonal perovskites with multiple functional properties, J. Mater. Chem. C 7 (2019) 10008–10018, https://doi.org/10.1039/C9TC03543E.
[49] S. Burger, K. Hemmer, D.C. Mayer, P. Vervoorts, D. Daisenberger, J.K. Zaręba, G. Kieslich, Designing geometric degrees of freedom in ReO 3 -type coordination polymers, Adv. Funct. Mater. (2022), 2205343, https://doi.org/10.1002/adfm.202205343.